


Structure, optical properties, and photocatalytic activity of $\alpha\text{-Ag}_2\text{W}_{0.75}\text{Mo}_{0.25}\text{O}_4$

 The corrections made in this section will be reviewed and approved by a journal production editor.

M.D. [Penha](#)^a, A.F. [Gouveia](#)^b, M.M. [Teixeira](#)^a, R.C. [de Oliveira](#)^c, M. [Assis](#)^a, J.R. [Sambrano](#)^c, F. [Yokaichya](#)^d, C.C. [Santos](#)^a, R.F. [Gonçalves](#)^e, M. [Siu Li](#)^f, M.A. [San-Miguel](#)^b, J. [Andrés](#)^{g,*} andres@qfa.uji.es, E. [Longo](#)^a

^aCDMF, Federal University of São Carlos, P.O. Box 676, São Carlos 13565-905, Brazil

^bInstitute of Chemistry, State University of Campinas, Unicamp, 13083-970, Campinas, SP, Brazil

^cModeling and Molecular Simulations Group, São Paulo State University, UNESP, Bauru, SP, Brazil

^dHelmholtz-Zentrum-Berlin, Berlin, 14109, Germany

^eUFCat, Federal University of Catalão, SetorUniversitário, 75704-020 Catalão, Brazil

^fIFSC, University of São Paulo, P.O. Box 369, 13560-970 São Carlos, Brazil

^gDepartament of Analytical and Physical Chemistry, University Jaume I, Castelló 12071, Spain

*Corresponding author.

Abstract

This article describes the synthesis of $\alpha\text{-Ag}_2\text{W}_{0.75}\text{Mo}_{0.25}\text{O}_4$ using a coprecipitation method followed by microwave irradiation for different times. The samples were characterized using X-ray and neutron diffractions with Rietveld refinement, Raman spectroscopy, X-ray fluorescence, and ultraviolet-visible diffused reflectance spectroscopy, as well as by photoluminescence emissions. To complement and rationalize the experimental results, first-principles calculations were performed. The formation and growth of metallic Ag nanoparticles on the surfaces of $\alpha\text{-Ag}_2\text{W}_{0.75}\text{Mo}_{0.25}\text{O}_4$ were studied by transmission electron microscopy and energy dispersive X-ray spectroscopy. Results show that $\alpha\text{-Ag}_2\text{W}_{0.75}\text{Mo}_{0.25}\text{O}_4$ samples obtained correspond to $\alpha\text{-Ag}_2\text{WO}_4/\beta\text{-Ag}_2\text{MoO}_4$ heterostructure, and the posterior microwave irradiation favors the process of substituting W by Mo, with subsequent formation of a solid solution. Photocatalytic tests were performed to verify the photocatalytic efficiency against the Rhodamine B. Photoluminescence emissions and photocatalytic results showed that the samples obtained at the longest microwave irradiation time promoted the formation of structural defects and enhanced the material properties.

Keywords: A. inorganic compounds; B. optical properties; C. neutron diffraction; D. catalytic properties

1 Introduction

Among the Ag-based materials, special attention is paid to Ag_2WO_4 and Ag_2MoO_4 because they can be used in a wide range of applications including gas-sensing, photo-switches, luminescence, antimicrobial agents, catalyst for dye degradation and water splitting, and so on [1–22]. Even the construction of composite photocatalysts involving Ag_2WO_4 , such as $\text{AgCl}/\text{Ag}_2\text{WO}_4$ [23], $\text{Ag}_2\text{WO}_4/\text{AgX}$ ($X = \text{Cl}, \text{Br}, \text{I}$) [24] and $\text{TiO}_2/\text{Ag}_2\text{WO}_4/\text{AgBr}$ [25] has been extensively proved to be an efficient method to enhance the photocatalytic efficiency under visible light.

Various methods have been reported in the literature to synthesize these tungstate/molybdate materials, such as impregnation [26,27], peptization [28,29], spray pyrolysis [30], deposition–precipitation [31], electrodeposition [32,33], sol-gel [34], hydrothermal reactions [35], solid state [36], and microwave radiation [37]. In this context, it is interesting to develop easy methods for synthesizing these materials under mild conditions. The coprecipitation (CP) method, followed by microwave irradiation, is an attractive protocol for synthesizing these materials. This strategy can offer important advantages, such as a short reaction time (e.g., within minutes), desired products with high purity and high yield, rapid heating, and low reaction temperature, because of the much lower reaction temperatures involved. It can also provide access to metastable phases, homogeneous thermal transmission, and lower aggregation levels [38–42].

Recently, the authors' research group synthesized $\alpha\text{-Ag}_2\text{W}_{0.50}\text{Mo}_{0.50}\text{O}_4$ crystals by using the CP method and posterior microwave hydrothermal treatment. This material displays photoluminescence (PL) emissions with higher intensities than those of single-structured $\alpha\text{-Ag}_2\text{WO}_4$. In addition, real-time *in-situ* formation and growth of Ag nanoparticles (NPs) on $\alpha\text{-Ag}_2\text{W}_{0.5}\text{Mo}_{0.5}\text{O}_4$ crystals using an accelerated electron beam under high *vacuum* were reported [43]. However, to date there have been no studies on the structure, optical properties, and photocatalytic activity of these systems. Based on the above considerations, this work is intended to complement previous studies and encourage the investigation of $\alpha\text{-Ag}_2\text{WO}_4$ with a higher concentration of Mo on the crystals and a W/Mo molar ratio of 3, forming $\alpha\text{-Ag}_2\text{W}_{0.75}\text{Mo}_{0.25}\text{O}_4$, by using a CP method followed by microwave irradiation for different processing times. The structure and optical properties were investigated by X-ray (XRD) and neutron diffractions with Rietveld refinement, Raman spectroscopy, X-ray fluorescence (XRF), field-emission scanning electron microscopy (FE-SEM), and ultraviolet-visible diffused reflectance spectroscopy (UV-vis DRS), as well as by photoluminescence emissions. The photocatalytic activity was investigated against the organic dye Rhodamine B (RhB). In addition, the formation and growth of metallic Ag NPs on the surfaces of $\alpha\text{-Ag}_2\text{W}_{0.75}\text{Mo}_{0.25}\text{O}_4$ crystals were studied by transmission electron microscopy (TEM), and energy-dispersive X-ray (EDX) spectroscopy.

Understanding the analogies between the experimental and the simulated scenarios implies new strategies for the rational comprehension of the formation processes of $\alpha\text{-Ag}_2\text{W}_{0.75}\text{Mo}_{0.25}\text{O}_4$ crystals, as well as the Ag NPs on their surfaces induced by electron beam irradiation. In this way, computational simulations based on density functional theory (DFT) were performed to complement and rationalize the experimental results, in particular, the local structure and optical properties. The present work aims to accomplish five goals: (i) to determine the nature of as-synthesized $\alpha\text{-Ag}_2\text{W}_{0.75}\text{Mo}_{0.25}\text{O}_4$ samples, (ii) how the formation of $\alpha\text{-Ag}_2\text{W}_{0.75}\text{Mo}_{0.25}\text{O}_4$ and the corresponding process of substituting W by Mo takes place, and (iii) what effect the microwave irradiation has, (iv) to find a correlation among structure, optical properties, and photocatalytic activity, and (v) to study the evolution behavior and growth mechanisms of Ag NPs induced by an electron beam. The results presented here demonstrate the great potential of combining experimental and theoretical measurements to explore and

contribute to a better understanding of semiconducting materials, based on tungstates and molybdates, and they mark another step toward next-generation semiconductors as alternatives to those commonly used at present.

This paper contains three more sections. In the next section, the experimental details are given (synthesis, characterization, photocatalytic measurements, and the computational methods and model systems). In Section 3, the results are presented and discussed. The main conclusions are summarized in Section 4.

2 Experimental details

2.1 Synthesis of $\alpha\text{-Ag}_2\text{W}_{0.75}\text{Mo}_{0.25}\text{O}_4$

A sample of $\alpha\text{-Ag}_2\text{W}_{0.75}\text{Mo}_{0.25}\text{O}_4$ was prepared by a CP method at 95 °C, followed by microwave irradiation for different reaction times. First, 0.75 mmol of sodium tungstate dihydrate ($\text{Na}_2\text{WO}_4 \cdot 2\text{H}_2\text{O}$, 99.5% purity, Aldrich) was dissolved in 50 mL of distilled water. Then, 0.25 mmol of sodium molybdate dihydrate ($\text{Na}_2\text{MoO}_4 \cdot 2\text{H}_2\text{O}$, 99.5% purity, Aldrich) was added and stirred magnetically at 95 °C for 10 min. Separately, 1 mmol of silver nitrate (AgNO_3 , 99% purity, Aldrich) was dissolved in 30 mL of distilled water at 95 °C. Silver nitrate solution was then added to the mixture (tungstate/molybdate) to form a homogeneous greenish-yellow precipitate. The resulting suspensions were transferred to a Teflon autoclave, which was sealed and placed in the microwave-assisted hydrothermal system. The reaction mixture was treated by heating at 140 °C for 2, 4, 8, and 16 min, using 2.45-GHz microwave radiation with a maximum power of 800 W. The autoclave was then kept at room temperature. The resulting greenish-yellow products were washed with distilled water followed by acetone to remove the ions remaining in the product and finally dried in a conventional furnace at 50 °C for 6 h.

2.2 Characterization

The crystals obtained were structurally characterized by X-ray diffraction (XRD) and neutron diffraction (ND) using the fine resolution powder diffractometer (FIREPOD-E9) at Helmholtz-Zentrum-Berlin, Germany [44]. The refinement routine adopted the 2θ range from 5° to 110° with a scanning rate of 0.01°min⁻¹. X-ray fluorescence (XRF) spectrometry was performed by EDX-720 (Shimadzu). Raman spectroscopy was recorded with a Bruker-RFS 100 (Germany). The morphologies of the samples were observed with field-emission scanning electron microscopy (FE-SEM). Ultraviolet-visible diffusion reflectance spectroscopy (UV-vis DRS) spectra were recorded using a Varian spectrophotometer (Varian, Cary 5 G model). PL measurements were performed using a Monospec 27 monochromator (Thermal Jarrel Ash, USA) coupled to an R446 photomultiplier (Hamamatsu, Japan). All PL measurements were taken at room temperature. More details about the characterization can be found in the Supplementary Material (SM).

2.3 Photocatalytic measurements

The photocatalytic activity was observed by photodegradation of Rhodamine B (RhB) dye in aqueous solution, at room temperature, under ultraviolet (UV) light irradiation. The photocatalytic system was equipped with six UV lamps (Light Sources INC G15/T8, 15 W ($\lambda_{\text{max}} = 254$ nm) and maintained at 20 °C with water circulation. The experimental procedure is consolidated in the literature [3,45,46] and more details can be found in the SM. Scavenger tests were performed using the p-benzoquinone (BQ) (Alfa-Aesar, 98%), ammonium oxalate monohydrate (AO) (Sigma-Aldrich, 99%), and tert-butyl alcohol (TBA) (Sigma-Aldrich, 99.5%).

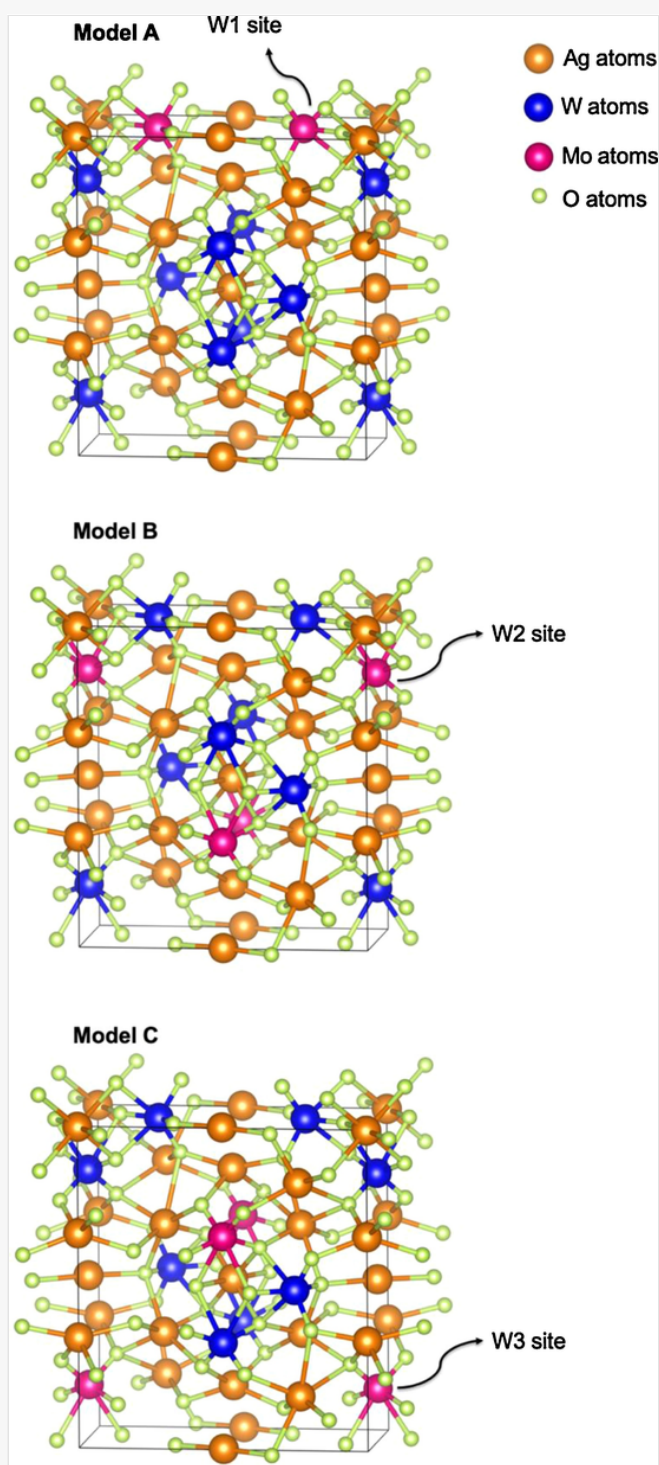
2.4 Computational methods and model systems

All calculations for the $\alpha\text{-Ag}_2\text{W}_{0.75}\text{Mo}_{0.25}\text{O}_4$ were performed with the CRYSTAL14 software package [47] and the details can be found in the SM. The Raman modes and their corresponding frequencies were calculated using numerical second derivatives of total energies, as implemented in the CRYSTAL14 package [47].

In the $\alpha\text{-Ag}_2\text{WO}_4$ structure, there are three different W-sites. To study the structural and electronic properties of $\alpha\text{-Ag}_2\text{W}_{0.75}\text{Mo}_{0.25}\text{O}_4$, three theoretical models with 25% Mo were selected: (i) model A replacing W1 by Mo, (ii) model B replacing W2 by Mo, and (iii) model C replacing W3 by Mo, as illustrated in Fig. 1. To evaluate the relative stability of each substitution, the total energies of the Mo replacement in the $\alpha\text{-Ag}_2\text{WO}_4$ were compared. The band structure and density of states (DOS) of $\alpha\text{-Ag}_2\text{W}_{0.75}\text{Mo}_{0.25}\text{O}_4$ were calculated and constructed along the appropriate high-symmetry directions of the corresponding irreducible Brillouin zone.

alt-text: Fig. 1

Fig. 1



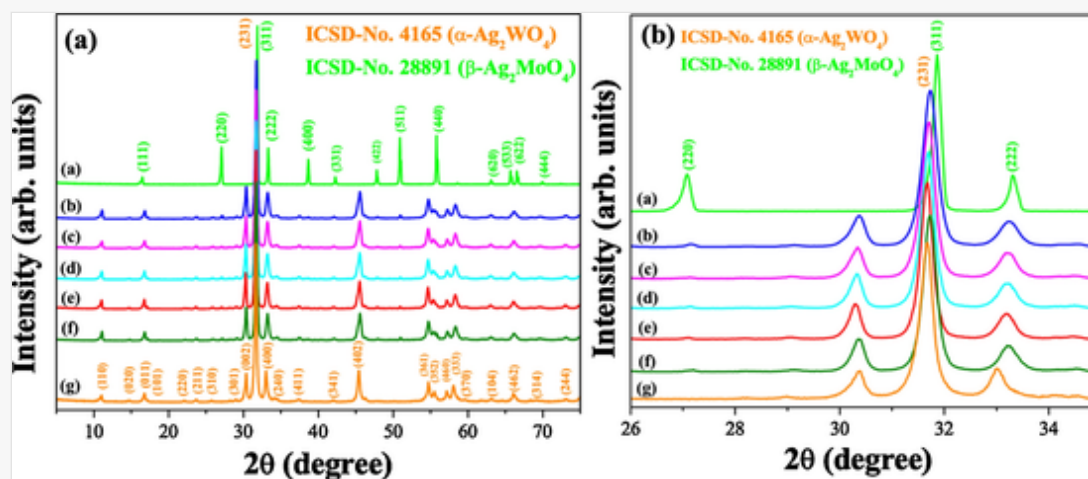
3 Results and discussion

3.1 Structural evolution of $\alpha\text{-Ag}_2\text{W}_{0.75}\text{Mo}_{0.25}\text{O}_4$

The XRD method was used to identify the structural organization at long range, the phase purity, and the crystalline structure of the samples. Fig. 2a shows the XRD patterns of the samples synthesized by the CP method and submitted to microwave irradiation at 140 °C for different reaction times. The diffraction peaks are in good agreement with those reported for $\alpha\text{-Ag}_2\text{WO}_4$ and $\beta\text{-Ag}_2\text{MoO}_4$ in the Inorganic Crystal Structure Database (ICSD) N° 4165 and N° 28892, respectively. $\alpha\text{-Ag}_2\text{WO}_4$ has an orthorhombic structure belonging to the $Pn2n$ group and lattice parameters $a = 10.878$ Å, $b = 12.009$ Å, $c = 5.895$ Å and angles $\alpha = \beta = \gamma = 90^\circ$. $\beta\text{-Ag}_2\text{MoO}_4$ has a cubic spinel structure belonging to the $Fd\bar{3}m$ group and lattice parameters $a = b = c = 9.3170$ Å and angles $\alpha = \beta = \gamma = 90^\circ$. For a better observation of the peaks, a zoom was performed between 26° and 35° , and can be seen in Fig. 2b. The structural order/disorder effects at long range can be analyzed by the full width at half maximum (FWHM) of the most intense peak of the XRD patterns, related to the plane (231) of $\alpha\text{-Ag}_2\text{WO}_4$. The sample obtained by the CP method showed an FWHM value of 0.54° , while the sample obtained after microwave irradiation had a value between 0.33° and 0.31° , showing a higher degree of crystallinity with respect to that obtained using the CP method.

alt-text: Fig. 2

Fig. 2




(a) XRD of (a) $\beta\text{-Ag}_2\text{MoO}_4$ and (g) $\alpha\text{-Ag}_2\text{WO}_4$ crystals prepared at 140 °C for 16 min by microwave irradiation, and $\alpha\text{-Ag}_2\text{W}_{0.75}\text{Mo}_{0.25}\text{O}_4$ crystals processed by the (b) CP method and by microwave irradiation for different times: (c) 2 min, (d) 4 min, (e) 8 min, (f) 16 min. (b) XRD approximation between 41° and 52° .

From the analysis of the XRD data, it is possible to conclude that the $\alpha\text{-Ag}_2\text{WO}_4$ structure is the main component, as can be seen in Fig. 2a and b, but there is also the presence of an additional phase, which corresponds to $\beta\text{-Ag}_2\text{MoO}_4$. Through the Rietveld refinement using the XRD technique, it was possible to identify the percentage of $\beta\text{-Ag}_2\text{MoO}_4$ and $\alpha\text{-Ag}_2\text{WO}_4$ present in each sample, obtained at different times of synthesis; the values are shown in Table 1. The values of the statistical parameters (R_{Bragg} and χ^2) and weight fraction of $\alpha\text{-Ag}_2\text{WO}_4$ and of $\beta\text{-Ag}_2\text{MoO}_4$ results obtained by the Rietveld refinement using the XRD technique for each sample are also shown in Table 1. Very recently, Gualtieri et al. [48] point out that with a

modern diffractometer and with an adequate data collection strategy, the signal/noise ratio should be good enough to detect crystalline phases even with concentration of 0.5–1 wt%. Therefore, the weight percentage value for α -Ag₂WO₄ and β -Ag₂MoO₄ samples obtained at 8 and 16 min are 99% and 1% and 1%, respectively.

alt-text: Table 1

Table 1

 The table layout displayed in this section is not how it will appear in the final version. The representation below is solely purposed for providing corrections to the table. To preview the actual presentation of the table, please view the Proof.

Parameters obtained by Rietveld refinement of the α -Ag₂W_{0.75}Mo_{0.25}O₄ samples.

Sample	R_{Bragg} ($\times 100$)	χ^2	R_{wp} ($\times 100$)	R_{p} ($\times 100$)	Weight fraction (%) α -Ag ₂ WO ₄	Weight fraction (%) β -Ag ₂ MoO ₄
CP ^a	6.2	2.7	8.1	5.9	97.0	3.0
2 min ^b	4.2	2.8	8.1	6.1	92.4	7.6
4 min ^b	6.4	2.8	6.9	5.6	92.9	7.1
8 min ^b	5.2	2.4	6.7	5.6	99.0	1.0
16 min ^b	8.8	2.7	6.9	5.6	99.0	1.0

Table Footnotes

^a CP method without posterior microwave irradiation.

^b CP method with posterior microwave irradiation.

This is the step in which the formation of the heterostructure took place, and it can be observed that the amount of α -Ag₂WO₄ and β -Ag₂MoO₄ formed varies with the synthesis time. Moreover, a greater quantity of β -Ag₂MoO₄ is expected to be formed, since 25% of Mo (in relation to the amount of W) was added in the synthesis. This result indicates that the solid solution may also have formed simultaneously to the heterostructure. In order to identify whether a solid solution has formed, Rietveld refinement was performed on the results obtained by using both X-ray and neutron diffraction techniques. The Rietveld refinement plots for samples processed by the CP method and submitted to microwave irradiation at 140 °C for different reaction times were obtained by means of the TOPAS program [49], and the corresponding results are presented in Figure SM-1.

Using the Rietveld refinement technique, it is possible to determine the percentage of W and Mo atoms that can occupy the three positions of W on the α -Ag₂WO₄ crystal lattice. Therefore, in this work, Rietveld refinements using X-ray and neutron diffractions were used to determine those values, the results being shown in Table SM-1.

The results presented in Tables 1 and 2 highlights the formation of a solid solution in which some Mo cations replace W cations in the crystalline lattice of the α -Ag₂WO₄ structure, simultaneously to the formation of the heterostructure.

The combination of the results obtained by X-ray and neutron diffractions confirms the crystalline structure. The compound obtained by CP has a structure with a high density of defects and an undefined solid solution, and heterostructure. Microwave irradiation, as a function of time, organizes the crystalline structure, reducing tensions and reorganizing the W and Mo cations in the most stable atomic positions. This fact is evidenced by the decrease in the heterostructure concentration, and the increase in the solid solution, which reaches a maximum at the longest time of microwave irradiation (16 min). Therefore, from the results presented in Tables 1 and 2, it can be seen that with the increase in the microwave irradiation time, the formation of solid solution is favored, which shows that a long reaction time in turn favors the process of substitution of W by Mo cations. This can be associated with the effect of the microwave irradiation that intensified the continuous crystallization–dissolution–recrystallization processes, as well as the effective collision rates between the small microcrystals. This result can only be observed by combining X-ray and neutron diffraction techniques. On the other hand, it is observed that for the system to increase its symmetry, there is a random transfer between the tungsten and molybdenum positions in the crystalline network.

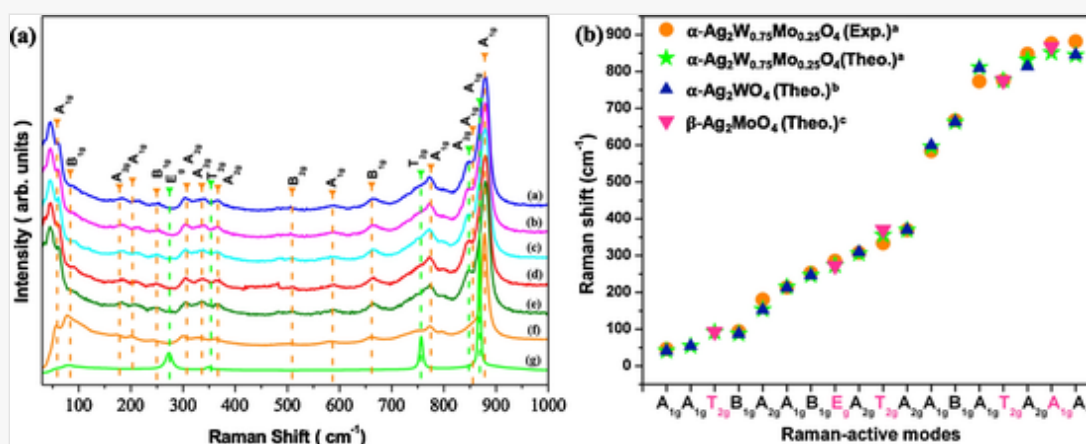
The elemental analysis of the amount of Mo and W present in each sample was performed by XRF spectrometry, as shown in Table SM-2. The composition of the Mo cations was close to the nominal values of 9% by weight, which corresponds to 25%. Therefore, it was possible to confirm that α - $\text{Ag}_2\text{W}_{0.75}\text{Mo}_{0.25}\text{O}_4$ samples were formed.

3.2 Raman peak assignments and vibrational analysis

Raman spectroscopy was used to analyze the characteristic modes of the α - $\text{Ag}_2\text{W}_{0.75}\text{Mo}_{0.25}\text{O}_4$ structure, as well as the short-range structural order/disorder effects. Fig. 3 shows the Raman spectra obtained both experimentally and theoretically for α - $\text{Ag}_2\text{W}_{0.75}\text{Mo}_{0.25}\text{O}_4$, in the range 30–1000 cm^{-1} , and they are assigned according to the related compounds α - Ag_2WO_4 [39,50] and β - Ag_2MoO_4 [51].

alt-text: Fig. 3

Fig. 3



(a) Raman spectra of the α - $\text{Ag}_2\text{W}_{0.75}\text{Mo}_{0.25}\text{O}_4$ obtained by the (a) CP method, and with microwave irradiation at different times, at: (b) 2 min, (c) 4 min, (d) 8 min, and (e) 16 min. α - Ag_2WO_4 (f) and β - Ag_2MoO_4 (g) crystals. (b) Correlation between of the experimental and theoretical Raman spectra of α - $\text{Ag}_2\text{W}_{0.75}\text{Mo}_{0.25}\text{O}_4$ obtained by the CP method (^aThis work; ^bLongo et al. [48]; ^cGouveia et al. [49]).

To compare the Raman modes of the α - $\text{Ag}_2\text{W}_{0.75}\text{Mo}_{0.25}\text{O}_4$ sample with the pure structures (α - Ag_2WO_4 and β - Ag_2MoO_4), the Raman spectra of all structures are shown in Fig. 3 (a) to follow the evolution of the

experimental samples. The Raman spectra of $\alpha\text{-Ag}_2\text{WO}_4$ can be classified into (a) internal modes, and (b) external modes, as reported in the literature [2,52–54].

Table SM-3 and Fig. 3 (b) show a variation in the positions of the Raman modes for $\alpha\text{-Ag}_2\text{W}_{0.75}\text{Mo}_{0.25}\text{O}_4$, in relation to precursor samples. Such a variation could be associated with structural distortions in the $[\text{AgO}_x]$ ($x = 2, 4, 6,$ and 7), $[\text{WO}_6]$, and $[\text{MoO}_4]$ clusters, as the constituent building blocks of $\alpha\text{-Ag}_2\text{WO}_4$ and $\beta\text{-Ag}_2\text{MoO}_4$. In addition, successive shifts in the modes also indicate a random substitution of the Mo atoms at the W site in the crystal lattice.

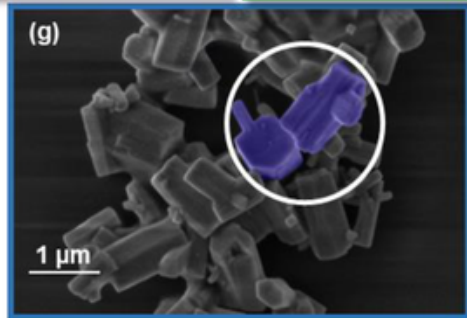
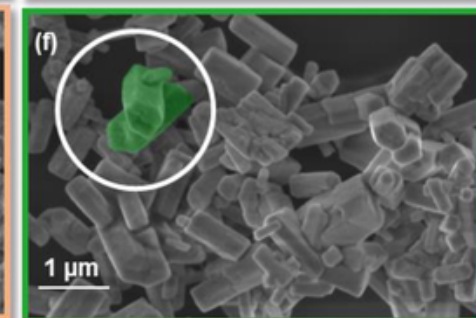
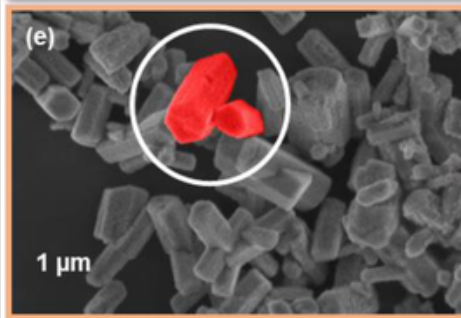
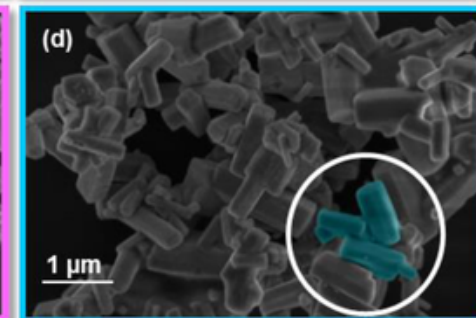
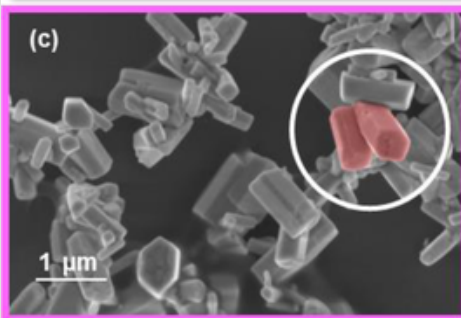
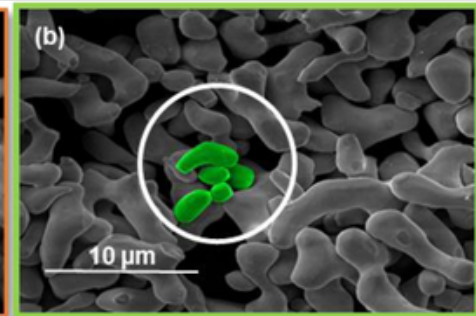
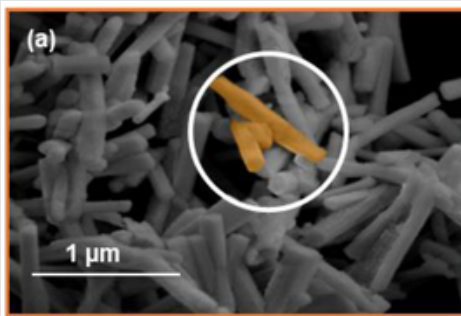
As in the XRD analysis, the FWHM was measured at the -880 cm^{-1} band, used with the order/disorder degree at a short range. A decrease in the FWHM values, $31.5, 31.4, 31.2,$ and 30.7 cm^{-1} was observed for the $\alpha\text{-Ag}_2\text{W}_{0.75}\text{Mo}_{0.25}\text{O}_4$ samples obtained by microwave irradiation at different times (2, 4, 8, and 16 min, respectively), as compared with the sample obtained by the CP method, 33.2 cm^{-1} . A lower degree of short-range disorder was observed for the $\alpha\text{-Ag}_2\text{W}_{0.75}\text{Mo}_{0.25}\text{O}_4$ samples irradiated by microwave than for the sample obtained by the CP method. Thus, the CP sample had a higher degree of short-range structural disorder in the $[\text{WO}_6]$ and $[\text{MoO}_4]$ clusters.

3.3 Surface structure and morphology of $\alpha\text{-Ag}_2\text{W}_{0.75}\text{Mo}_{0.25}\text{O}_4$

Fig. 4 (a, b) show the micrographs of pure $\alpha\text{-Ag}_2\text{WO}_4$ and $\beta\text{-Ag}_2\text{MoO}_4$ samples. Fig. 4 (c–g) display the morphology of the $\alpha\text{-Ag}_2\text{W}_{0.75}\text{Mo}_{0.25}\text{O}_4$ samples obtained by CP and submitted to microwave irradiation at $140\text{ }^\circ\text{C}$ for different reaction times (2–16 min). An analysis of the images shows that $\alpha\text{-Ag}_2\text{W}_{0.75}\text{Mo}_{0.25}\text{O}_4$ microcrystals have hexagonal rod-like morphologies with elongated irregular shapes.

alt-text: Fig. 4

Fig. 4



FE-SEM of the α -Ag₂WO₄ (a) and β -Ag₂MoO₄ (b) crystals. The α -Ag₂W_{0.75}Mo_{0.25}O₄ synthesized by microwave irradiation at 140 °C for: (c) 2 min, (d) 4 min, (e) 8 min, (f) 16 min, and by the (g) CP method.

In previous research [3,46] a map of available morphologies of the α -Ag₂WO₄ crystals was obtained by using the Wulff construction, and it was found that, under equilibrium conditions, hexagonal rod-like morphologies with elongation along the [010] direction can be detected.

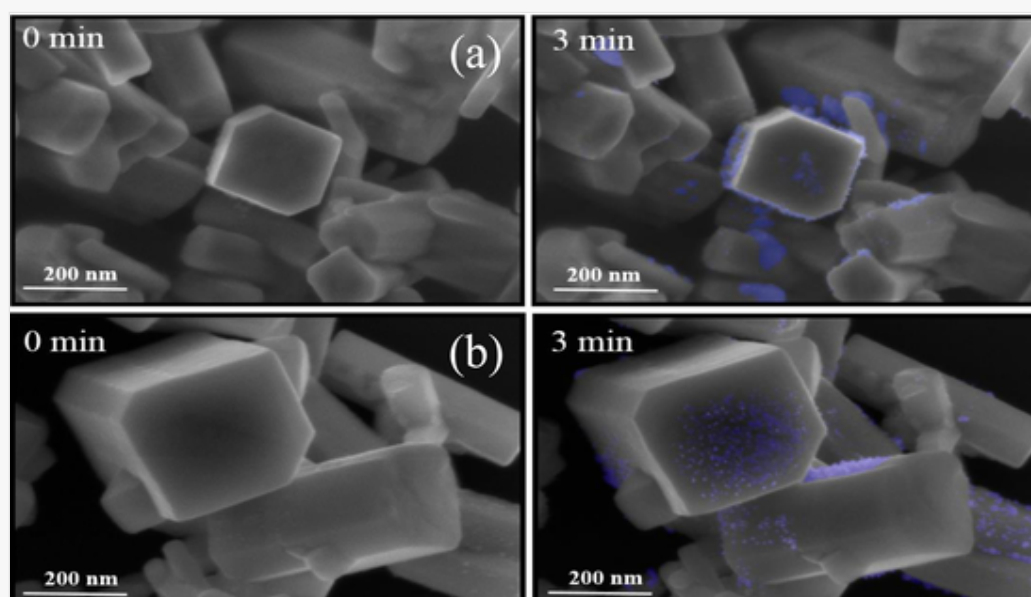
For α -Ag₂W_{0.75}Mo_{0.25}O₄, the increase in the reaction time of microwave irradiation cannot change the morphology. However, the distribution of the average size decreases by almost 60% as a function of the microwave irradiation time during the synthesis (see Figure SM-2). This decrease in size is due to the recrystallization process along the synthesis.

Recently, real-time in-situ nucleation and Ag NPs growth processes on different silver-based semiconductors, such as α - and β -Ag₂WO₄ [46,55], β -Ag₂MoO₄ [38,56], Ag₃PO₄ [57], Ag₂(W_{1-x}Mo_x)O₄ [43], and β -AgVO₃ [58], were reported. They were driven by accelerated electron beam irradiation from an electron microscope under a high vacuum. The reasons for this phenomenon have been discussed in recent publications [50,55,56,59]. The processes of Ag NP formation and growth on the α -Ag₂W_{0.75}Mo_{0.25}O₄ surface were studied.

The onset of Ag NP nuclei on the surface of the α -Ag₂W_{0.75}Mo_{0.25}O₄ samples was observed in the FE-SEM images (Fig. 5 and SM-3) as soon as the samples began to be analyzed. An FE-SEM image of the rod-like crystals was acquired after a rapid approach and focus adjustment (time zero), as shown in Fig. 5 (a) and (b) (the reaction times 4 to 16 min, shown in the Figure SM-3). After 3 min exposure to an electron beam under an accelerating voltage of 5 kV, the particle shows regions with Ag NPs on the surface of the particles. This image shows that, after a short exposure to the electron beam, there is a cluster of the reduction process, [AgO₆] clusters of β -Ag₂MoO₄, and [AgO₂]/[AgO₄] clusters of α -Ag₂WO₄ on the surface of the α -Ag₂W_{0.75}Mo_{0.25}O₄ system, giving rise to Ag NPs on the surface of the material [55,60].

alt-text: Fig. 5

Fig. 5

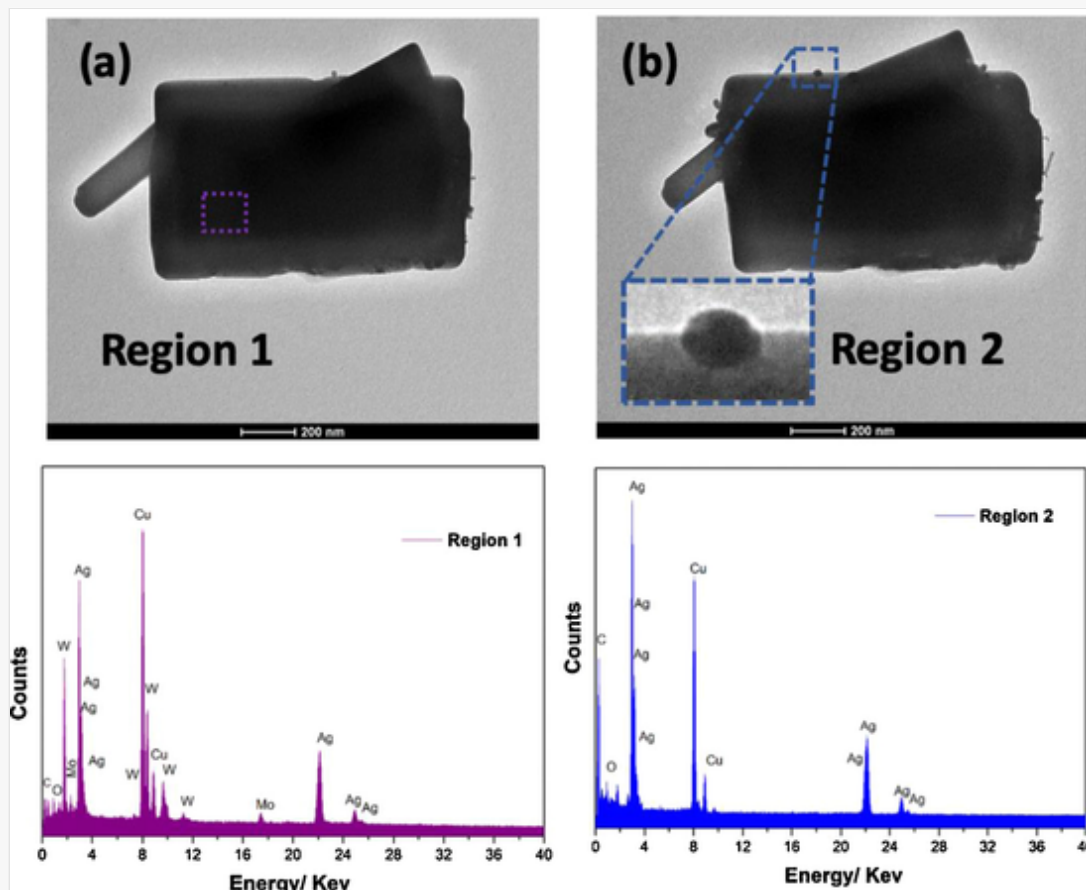


FE-SEM after a 3-min exposure to the electron beam (accelerated to 5 kV) of the scanning electron microscope α -Ag₂W_{0.75}Mo_{0.25}O₄ obtained by the CP method (a) and by microwave irradiation for 2 min (b).

To verify the growth of metallic Ag NPs on the $\alpha\text{-Ag}_2\text{W}_{0.75}\text{Mo}_{0.25}\text{O}_4$ surface, an EDX system coupled with a TEM microscope was used to analyze the samples, as shown in Fig. 6, making it possible to investigate the chemical composition and purity of the $\alpha\text{-Ag}_2\text{W}_{0.75}\text{Mo}_{0.25}\text{O}_4$ surface.

alt-text: Fig. 6

Fig. 6



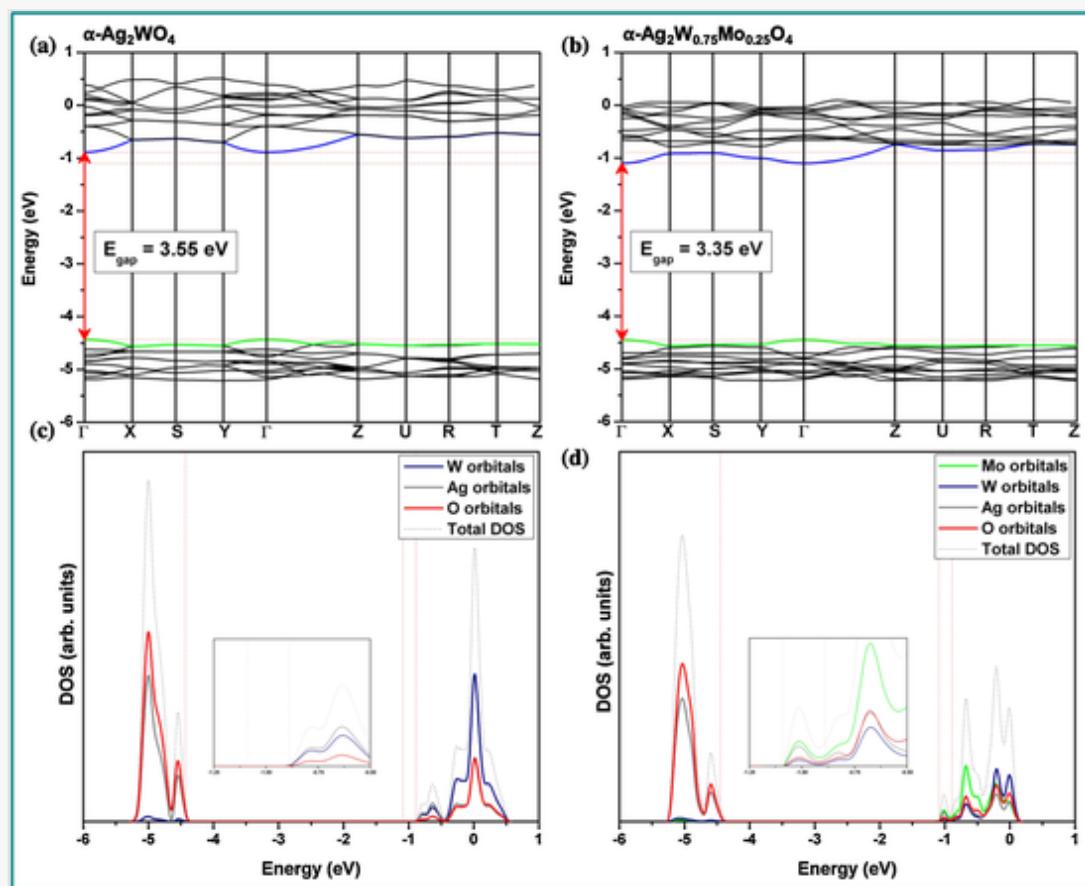
TEM images and EDX analyses of $\alpha\text{-Ag}_2\text{W}_{0.75}\text{Mo}_{0.25}\text{O}_4$ for 16 min of microwave irradiation: (a) before, and (c) after a 2-min exposure to the electron beam.

The $\alpha\text{-Ag}_2\text{W}_{0.75}\text{Mo}_{0.25}\text{O}_4$ samples were submitted to electron beam irradiation in the TEM microscope for 2 min, and distinct regions in the $\alpha\text{-Ag}_2\text{W}_{0.75}\text{Mo}_{0.25}\text{O}_4$ microparticles were focused on and selected for examination. Fig. 6 (a, b) correspond to the sample before and after irradiation, respectively. These two distinct regions (lilac and blue) were selected. Region 2 indicates the presence of Ag NPs, as evident from the EDX analysis. As expected, EDX results – Fig. 6 (b) in Region 2 – confirmed that the electron beam promoted the random growth of the metallic Ag NPs. Fig. 6 (a) (Region 1) indicates that the material is composed of Ag, W, Mo, and O, implying that $\alpha\text{-Ag}_2\text{W}_{0.75}\text{Mo}_{0.25}\text{O}_4$ was formed during the reaction once the Ag atoms migrated out of the matrix [38].

3.4 Band structure, density of states, and PL spectra

The electronic levels in $\alpha\text{-Ag}_2\text{W}_{0.75}\text{Mo}_{0.25}\text{O}_4$ were studied by means of theoretical calculations. The band structures of $\alpha\text{-Ag}_2\text{WO}_4$ and $\alpha\text{-Ag}_2\text{W}_{0.75}\text{Mo}_{0.25}\text{O}_4$ are presented in Fig. 7 (a, b), respectively, illustrating direct band gap values of 3.55 and 3.35 eV located at the Γ point of the Brillouin zone.

Fig. 7



Band structure and density of states for (a, c) $\alpha\text{-Ag}_2\text{WO}_4$ and (b, d) $\alpha\text{-Ag}_2\text{W}_{0.75}\text{Mo}_{0.25}\text{O}_4$, respectively.

In the $\alpha\text{-Ag}_2\text{W}_{0.75}\text{Mo}_{0.25}\text{O}_4$, a decrease in the optical band gap energy (E_{gap}) value was observed. A comparison of the two band structures shows that this decrease is caused by the creation of a new intermediate level between the valence band (VB) and the conduction band (CB), with these new levels located in the CB. To verify the atom or the group of atoms responsible for the creation of the new intermediate level, it is necessary to analyze the DOS.

Fig. 7 (c, d) show the DOS projected on Ag, W, Mo, and O atoms and the total DOS projected over all atoms in $\alpha\text{-Ag}_2\text{WO}_4$ and $\alpha\text{-Ag}_2\text{W}_{0.75}\text{Mo}_{0.25}\text{O}_4$, respectively. An analysis of the DOS in Fig. 7 (c, d) shows that the profile for the VB is almost the same for both structures, $\alpha\text{-Ag}_2\text{WO}_4$ and $\alpha\text{-Ag}_2\text{W}_{0.75}\text{Mo}_{0.25}\text{O}_4$, with a major contribution at the top of this band from the O 2p and Ag 4d orbitals. However, in the CB, the profile is not maintained, and the intensity of the density decreases in $\alpha\text{-Ag}_2\text{W}_{0.75}\text{Mo}_{0.25}\text{O}_4$. The contribution of the W cations is maintained, and the Mo cations are responsible for the decrease in the band gap value. The major contribution of the Mo cations appears in the region between -1.0 and -0.5 eV, which is prohibited for $\alpha\text{-Ag}_2\text{WO}_4$. Therefore, the bottom of the CB in the $\alpha\text{-Ag}_2\text{WO}_4$ is composed mainly of W 5d orbitals, while $\alpha\text{-Ag}_2\text{W}_{0.75}\text{Mo}_{0.25}\text{O}_4$ is formed by the contribution of the Mo 4d orbital.

The electronic properties are directly associated with the arrangement of the atoms in the crystalline structure. The synthesis method, as well as the temperature, the time employed, and the introduction of impurities, can modify this arrangement, causing a structural disorder at medium range and local bond distortions [51,61] in the $[\text{WO}_6]$ and $[\text{MoO}_4]$ clusters.

The theoretical E_{gap} values for all samples agree with the experimental E_{gap} values obtained, as in Figure SM-4. The pure $\alpha\text{-Ag}_2\text{WO}_4$ and $\beta\text{-Ag}_2\text{MoO}_4$ samples showed higher E_{gap} values than the $\alpha\text{-Ag}_2\text{W}_{0.75}\text{Mo}_{0.25}\text{O}_4$ samples, because of the density of the defects formed in the CB with the insertion of Mo atoms.

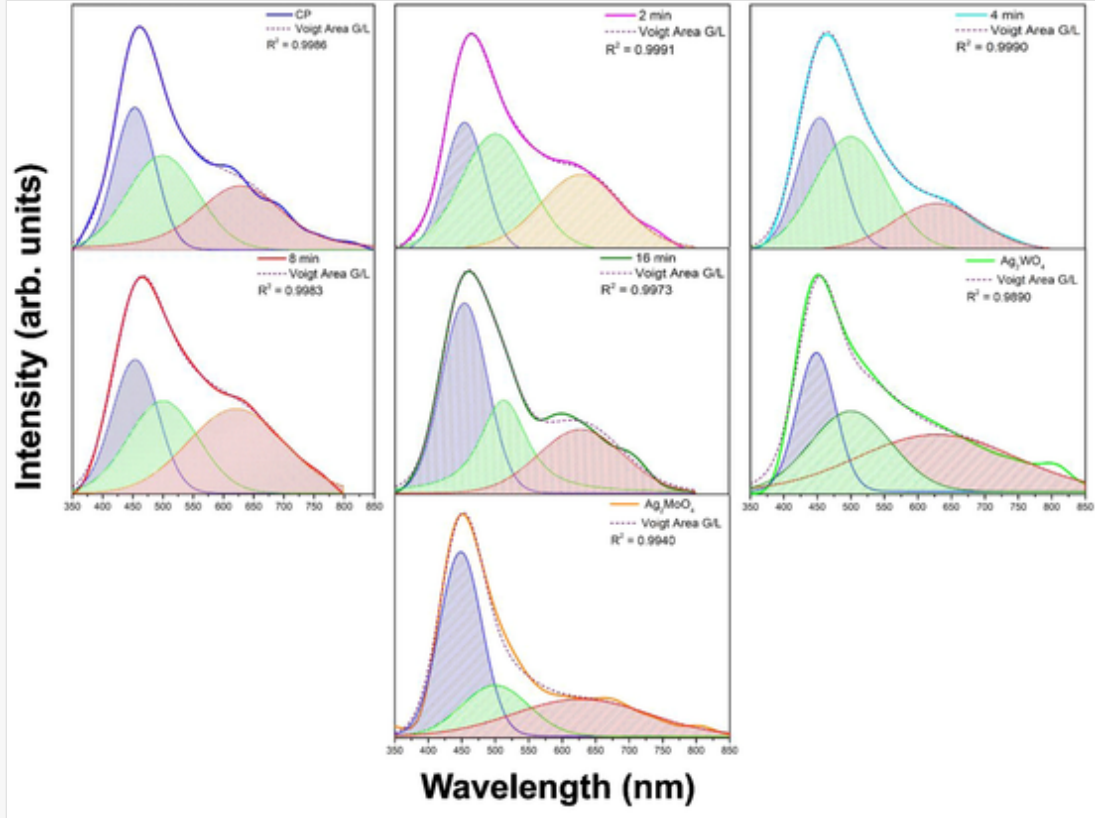
To characterize the types of defect present in the structure of the $\alpha\text{-Ag}_2\text{W}_{0.75}\text{Mo}_{0.25}\text{O}_4$ samples, PL measurements were performed, as shown in Figure SM-5. All samples showed broadband emission with a slight shift in the maximum emission center. The maximum emission center of all samples corresponds to electron transition between the VB ($2p$ levels of O atoms and $4d$ levels of Ag atoms) and CB ($5d$ levels of W and $4d$ Mo atoms) and agrees with the experimental E_{gap} values obtained, as in Figure SM-4. This is because the pure $\alpha\text{-Ag}_2\text{WO}_4$ and $\beta\text{-Ag}_2\text{MoO}_4$ samples had higher E_{gap} values, in agreement with the high energy of the maximum emission center, as shown in Figure SM-5 (a). The $\alpha\text{-Ag}_2\text{W}_{0.75}\text{Mo}_{0.25}\text{O}_4$ samples had lower E_{gap} values than the pure sample (Figure SM-4), in agreement with the maximum emission center being shifted for lower energy, as shown in Figure SM-5 (a).

A chromaticity diagram was made to determine whether there was a difference in the color emissions of all samples, because the samples had a similar PL profile, as seen in Figure SM-5 (b) and Table SM-4. All samples had different coordinates and CIE colors, and this is related to different luminescent centers, such as different defect energy levels present in the samples.

To characterize the emission centers and types of defect, the PL spectra were deconvoluted in three peaks (area of the Voigt function), centered in the blue region (454 nm, 2.73 eV), green region (500 nm, 2.48 eV), and red region (628 nm, 1.97 eV), as in Fig. 8. The emission in the blue region is related to VB-to-CB electron transition, and this more energetic transition of 2.73 eV is favored by distortions in the crystal lattice. The emission in the green region at 2.48 eV is attributed to shallow defects that are nearest to the CB, which is favored by distortion in the bond and angles of the $[\text{AgO}_x]$, $[\text{WO}_6]$, and $[\text{MoO}_4]$ clusters. The emission in the red region at 1.97 eV is related to deeper defects in the forbidden zone of the band gap [55], which is promoted by silver and oxygen vacancies in the samples [52].

alt-text: Fig. 8

Fig. 8



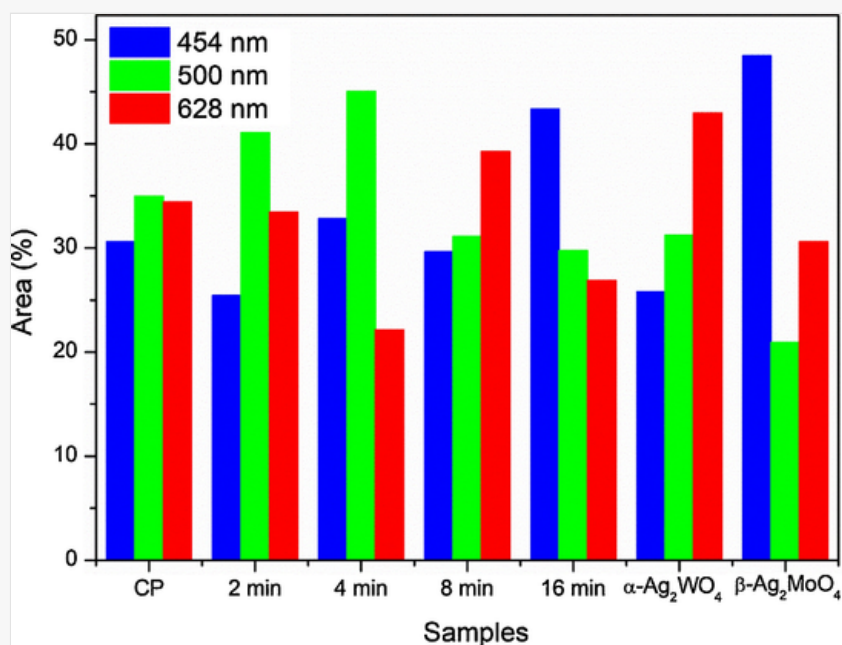
Deconvolution PeakFit of PL spectra for the $\alpha\text{-Ag}_2\text{W}_{0.75}\text{Mo}_{0.25}\text{O}_4$ sample obtained by the CP method, and processed at different times by a microwave hydrothermal system.

The contribution of each defect in the samples is shown in Fig. 9. Thus, the pure $\alpha\text{-Ag}_2\text{WO}_4$ sample exhibited a high percentage in the red region, which is deep defects, and the pure $\beta\text{-Ag}_2\text{MoO}_4$ sample showed a high percentage in the blue region, which corresponds to structural defects. For the $\alpha\text{-Ag}_2\text{W}_{0.75}\text{Mo}_{0.25}\text{O}_4$ samples, the one obtained by the CP method displayed an equilibrium in the emissions in the blue, green, and red regions, i.e., there was a balance in the structural, shallow, and deep defects in this sample. For the samples processed in the microwave system, a change in the emission centers could be observed as the reaction time changed. Thus, the variation in reaction times created different densities of defects in the structure that favored different emission centers in the samples. For the samples obtained at reaction times of 2 and 4 min, there was a favored emission in the green region of shallow defects. For the sample obtained at a reaction time of 8 min, the emission was

favored in the red region of deep defects, whereas, for the sample obtained with a long reaction time of 16 min, there was a higher percentage of emission in the blue region of structural defects. Therefore, the reaction time in the microwave system enhanced the order/disorder effect in the structure, associated with the crystallization–dissolution–recrystallization processes, to aid the process of substitution of W by Mo cations in the α - Ag_2WO_4 lattice, as observed in the Rietveld refinement (Table 1).

alt-text: Fig. 9

Fig. 9



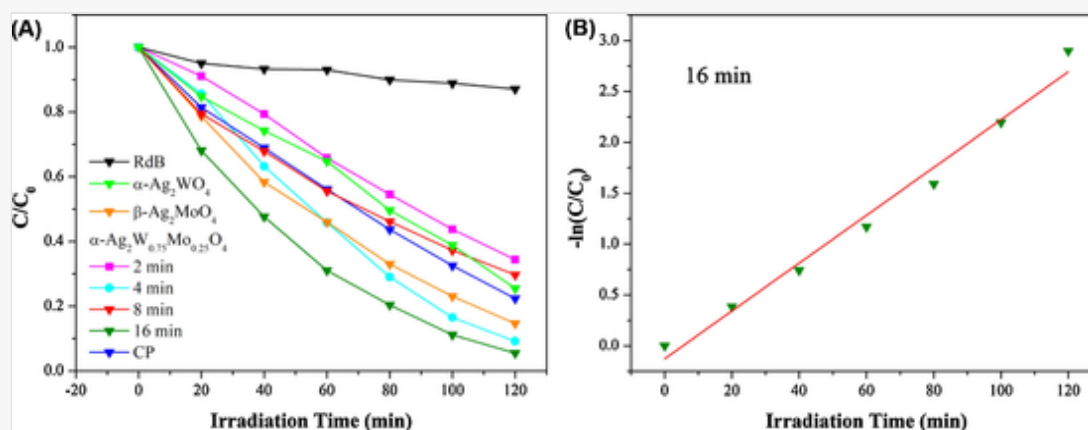
Area percentage of the PL spectra of the α - $\text{Ag}_2\text{W}_{0.75}\text{Mo}_{0.25}\text{O}_4$ obtained by the CP method and followed by microwave irradiation for different times.

3.5 Photocatalytic activity

The photocatalytic activity of the α - $\text{Ag}_2\text{W}_{0.75}\text{Mo}_{0.25}\text{O}_4$ samples was evaluated by the photodegradation of RhB in aqueous solution, in neutral pH, and under UV light irradiation. The adsorption–desorption equilibrium of the samples was analyzed after stirring in the dark for 20 min. The β - Ag_2MoO_4 sample showed an adsorption capacity in the dark, while the other samples did not show any appreciable alterations in the absorbance over time (Figure SM-6). The efficiency in the adsorption process did not remain for the α - $\text{Ag}_2\text{W}_{0.75}\text{Mo}_{0.25}\text{O}_4$ samples. This may be related to the change in surface area and morphology (Fig. 4), which can offer more active adsorption sites and centers of photocatalytic reaction. The photolysis experiment was carried out on the RhB solution containing no photocatalyst, the results showing the occurrence of relatively negligible degradation in the presence of UV light.

Fig. 10 (a) shows the photocatalytic activity for the α - Ag_2WO_4 , β - Ag_2MoO_4 , and α - $\text{Ag}_2\text{W}_{0.75}\text{Mo}_{0.25}\text{O}_4$ samples. The degradation percentage is shown as $\ln C/C_0$, where C is the concentration of RhB dye in a given time interval, and C_0 corresponds to the initial concentration of the dye. The degree of degradation was determined from the decrease in the characteristic absorption band of the RhB through a concentration calibration curve. It was clear that the absorption peaks at 554 nm, corresponding to RhB, decreased rapidly as the exposure time increased, thus indicating the decomposition of RhB and a significant reduction in concentration.

Fig. 10



(a) Photocatalytic degradation of RhB over pure $\alpha\text{-Ag}_2\text{WO}_4$, $\beta\text{-Ag}_2\text{MoO}_4$, and $\alpha\text{-Ag}_2\text{W}_{0.75}\text{Mo}_{0.25}\text{O}_4$ obtained by CP and submitted to a microwave irradiation. (b) the kinetics of RhB photocatalytic degradation over $\alpha\text{-Ag}_2\text{W}_{0.75}\text{Mo}_{0.25}\text{O}_4$ at 16 min of microwave irradiation.

The pure $\alpha\text{-Ag}_2\text{WO}_4$ and $\beta\text{-Ag}_2\text{MoO}_4$ samples showed a photodegradation of approximately 77% and 87% and 87% of RhB after UV light irradiation, respectively. It became evident that, for the activity of $\alpha\text{-Ag}_2\text{W}_{0.75}\text{Mo}_{0.25}\text{O}_4$, an improvement in the dye degradation process occurred, as in Fig. 10 (a). The sample processed in the microwave system for 16 min showed a high photocatalytic activity, and 95% of RhB degraded in 120 min after UV irradiation. In this sample, the dissolution and recrystallization process in the microwave system favored a higher percentage of insertion of Mo cations in the $\alpha\text{-Ag}_2\text{WO}_4$ lattice (Tables 1 and SM-1), which promoted higher structural disorder of the crystal lattice, and possibly favored the separation of charges – electron (e^-) and hole (h^\bullet) – thereby increasing the efficiency of the degradation. This effect is indicated by the high polarization that the Mo cations introduce in the structure of $\alpha\text{-Ag}_2\text{W}_{0.75}\text{Mo}_{0.25}\text{O}_4$, with concomitant formation of dipoles, quadrupoles, etc. in the material. Thus, these structural and electronic defects increased the photocatalytic activity of the $\alpha\text{-Ag}_2\text{W}_{0.75}\text{Mo}_{0.25}\text{O}_4$ samples.

RhB photodegradation curves with the pure $\alpha\text{-Ag}_2\text{WO}_4$, $\beta\text{-Ag}_2\text{MoO}_4$, and $\alpha\text{-Ag}_2\text{W}_{0.75}\text{Mo}_{0.25}\text{O}_4$ samples were adjusted by pseudo-first-order reaction kinetics (k') using Langmuir–Hinshelwood kinetics [62,63], described in the integrated Eq. (1), which considers the influence of the initial concentration of the solute on the rate of photocatalytic degradation of the compounds,

$$\ln \frac{C_0}{C} = kt$$

(1)

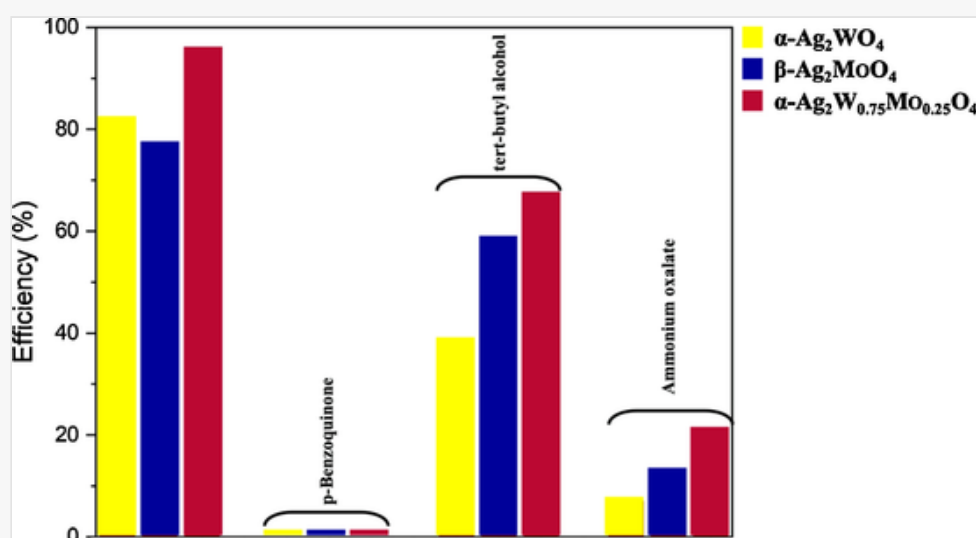
where k (min^{-1}) is the apparent rate constant that is affected by the dye concentration, and t is the time.

Fig. 10 (b) shows that photocatalytic degradation follows the pseudo-first order. The apparent velocity constant for all studied samples is determined from the inclinations of $\ln(C_0/C)$ versus the UV irradiation time, and the values obtained are listed in Table SM-5. The $\alpha\text{-Ag}_2\text{W}_{0.75}\text{Mo}_{0.25}\text{O}_4$ obtained in the reaction time of 16 min showed a high-speed constant of 0.023 min^{-1} , as in Table SM-5. Thus, the formation of $\alpha\text{-Ag}_2\text{W}_{0.75}\text{Mo}_{0.25}\text{O}_4$ was efficient to increase the photocatalytic activity of RhB compared with the pure $\alpha\text{-Ag}_2\text{WO}_4$, $\beta\text{-Ag}_2\text{MoO}_4$ samples.

To further explore the mechanism of RhB photodegradation, the free radical $O_2^{\cdot -}$, OH^{\cdot} , and h^{\cdot} trapping experiments were carried out to identify which reactive species are taking part in the degradation process. p-benzoquinone (BQ, $O_2^{\cdot -}$ quencher), tert-butyl alcohol (TBA, OH^{\cdot} quencher) and ammonium oxalate (AO, h^{\cdot} quencher) were added to the photocatalytic system. As shown in Fig. 11, the photodegradation activity was apparently suppressed with the presence of BQ, implying that $O_2^{\cdot -}$ plays an important role in the photodegradation process; by the other side, the addition of AO and TBA have minor effects on the degradation of RhB.

alt-text: Fig. 11

Fig. 11



The effects of various scavengers on the visible-light photodegradation of RhB for $\alpha\text{-Ag}_2\text{WO}_4$, $\beta\text{-Ag}_2\text{MoO}_4$, and $\alpha\text{-Ag}_2\text{W}_{0.75}\text{Mo}_{0.25}\text{O}_4$ obtained at 16 min of microwave hydrothermal irradiation.

4 Conclusions

A faster and greener CP approach, followed by microwave irradiation at different reaction times (2 to 16 min) has been demonstrated for the synthesis of $\alpha\text{-Ag}_2\text{W}_{0.75}\text{Mo}_{0.25}\text{O}_4$. X-ray and neutron diffraction with Rietveld refinement of the $\alpha\text{-Ag}_2\text{W}_{0.75}\text{Mo}_{0.25}\text{O}_4$ samples show that the $\alpha\text{-Ag}_2\text{WO}_4$ structure is the main component, with a small percentage of additional $\beta\text{-Ag}_2\text{MoO}_4$ phase, with the formation of an $\alpha\text{-Ag}_2\text{WO}_4/\beta\text{-Ag}_2\text{MoO}_4$ heterostructure. Moreover, the XRF measurements reveal that the long reaction time in the microwave irradiation favors the process of substitution of W by Mo, with subsequent formation of a solid solution with 25% of Mo in the structure. The Raman spectra show that the vibrational modes are in accordance with those of the tungstate and molybdate compounds. UV-vis DRS measures indicate that $\alpha\text{-Ag}_2\text{W}_{0.75}\text{Mo}_{0.25}\text{O}_4$ has good light absorption properties in the UV region. In addition, the decrease in E_{gap} values shows the formation of intermediate energy levels within the band gap because of the presence of Mo cations. The experimental results indicate that a crystallization–dissolution–recrystallization self-assembly growth mechanism associated with the microwave heating dominates the formation of a hexagonal rod-like morphology. First-principles calculations, at the DFT level, were performed. Geometries, energetics, structural parameters, and electronic properties (band structure and DOS) of $\alpha\text{-Ag}_2\text{W}_{0.75}\text{Mo}_{0.25}\text{O}_4$ were obtained and compared with available experimental data. The PL and photocatalysis results showed that the $\alpha\text{-Ag}_2\text{W}_{0.75}\text{Mo}_{0.25}\text{O}_4$ samples obtained at the longest time (16 min) of microwave irradiation promoted the formation of structural defects and enhanced the degradation process of RhB.

CRedit authorship contribution statement

M.D. Penha: Investigation, Methodology, Writing - original draft. **A.F. Gouveia:** Investigation, Methodology, Writing - original draft, Writing - review & editing. **M.M. Teixeira:** Investigation, Methodology, Writing - original draft. **R.C. de Oliveira:** Writing - review & editing. **M. Assis:** Investigation, Methodology, Writing - original draft. **J.R. Sambrano:** Supervision, Funding acquisition, Investigation, Writing - review & editing. **F. Yokaichya:** Investigation, Methodology, Writing - original draft. **C.C. Santos:** Investigation, Methodology, Writing - original draft. **R.F. Gonçalves:** Supervision, Investigation, Methodology, Writing - original draft. **M. Siu Li:** Investigation, Methodology, Writing - review & editing. **M.A. San-Miguel:** Supervision, Funding acquisition, Investigation, Writing - review & editing. **J. Andrés:** Conceptualization, Supervision, Writing - original draft, Writing - review & editing. **E. Longo:** Supervision, Funding acquisition, Investigation, Writing - review & editing.

Declaration of Competing Interest

The authors declare that they have no known competing financial interests or personal relationships that could have appeared to influence the work reported in this paper.

Acknowledgments

The authors acknowledge the financial support of agencies: **FAPEMA**, **CAPES** (PNPD – 1268069; Finance Code 001), **FAPESP** (2013/07296-2; 2016/23891-6; 2019/01732-1; 2019/08928-9), and **CNPq** (304531/2013-8). J.A. acknowledges Ministerio de Ciencia, Innovación y Universidades (Project No. PGC2018-094417-B-I00), and Universitat Jaume I (Project UJI-B2019-30).

Appendix A Supplementary data

Supplementary material related to this article can be found, in the online version, at doi:<https://doi.org/10.1016/j.materresbull.2020.111011>.

References



The corrections made in this section will be reviewed and approved by a journal production editor. The newly added/removed references and its citations will be reordered and rearranged by the production team.

- [1] Ng C.H.B., Fan W.Y., Crystengcomm 18 (2016) 8010–8019.
- [2] Lin Z., Li J., Zheng Z., Yan J., Liu P., Wang C., Yang G., ACS Nano 9 (2015) 7256–7265.
- [3] Macedo N.G., Gouveia A.F., Roca R.A., Assis M., Gracia L., Andrés J., Leite E.R., Longo E., J. Phys. Chem. C 122 (2018) 8667–8679.
- [4] Nobre F.X., Bastos I.S., dos Santos Fontenelle R.O., Júnior E.A.A., Takeno M.L., Manzato L., de Matos J.M.E., Orlandi P.P., de Fátima Souza Mendes J., Brito W.R., da Costa Couceiro P.R., ~~Ultrasonics sonochemistry~~. ~~Sonochem.~~ Ultrason. Sonochem. 58 (2019) 104620.

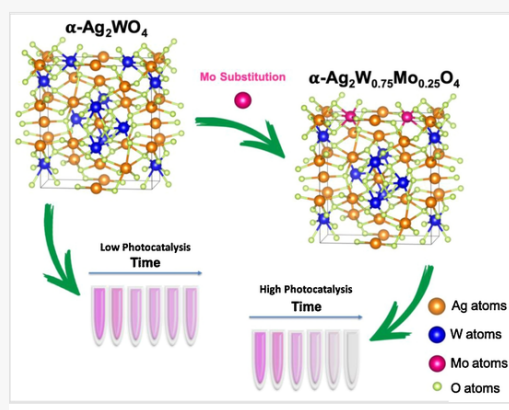
- [5] da Silva L.F., Catto A.C., Avansi W., Cavalcante L.S., Mastelaro V.R., Andres J., Aguir K., Longo E., *J. Alloys Compd.* 683 (2016) 186–190.
- [6] de Foggi C.C., de Oliveira R.C., Fabbro M.T., Vergani C.E., Andres J., Longo E., Machado A.L., *Cryst. Growth Des.* 17 (2017) 6239–6246.
- [7] Cheng L., Shao Q., Shao M., Wei X., Wu Z., *J. Phys. Chem. C* 113 (2009) 1764–1768.
- [8] Fodjo E.K., Li D.W., Marius N.P., Albert T., Long Y.T., ~~*Journal of Materials Chemistry A*~~, *Mater. Chem. A* 1 (2013) 2558–2566.
- [9] Li S.J., Hu S.W., Jiang W., Liu Y.P., Liu Y., Zhou Y.T., Mo L.Y., Liu J.S., ~~*Beilstein Journal of Nanotechnology*~~, *Nanotechnol. Beilstein J. Nanotechnol.* 9 (2018) 1308–1316.
- [10] Singh D.P., Sirota B., Talpatra S., Kohli P., Rebholz C., Aouadi S.M., ~~*Journal of Nanoparticle Research*~~, *Nanoparticle Res. J. Nanoparticle Res.* 14 (2012).
- [11] Wu G.Y., Xing W.N., ~~*Materials Technology*~~, *Technol. Mater. Technol.* 34 (2019) 292–300.
- [12] Pellissari C.V.G., Vergani C.E., Longo E., Pavarina A.C., Sanita P.V., Siqueira W.L., Jorge J.H., ~~*Journal of Nanomaterials*~~, *Nanomater. J. Nanomater.* 2020 (2020).
- [13] Bhattacharya S., Ghosh A., ~~*Physical Review B*~~, *Rev. B Phys. Rev. B* 75 (2007).
- [14] Nubla K., Sandhyarani N., ~~*Electrochimica Acta*~~, *Electrochim. Acta* (2020) 135942.
- [15] De Foggi C.C., De Oliveira R.C., Assis M., Fabbro M.T., Mastelaro V.R., Vergani C.E., Gracia L., Andrés J., Longo E., Machado A.L., ~~*Materials Science and Engineering: C*~~, *Sci. Eng. C Mater. Sci. Eng. C* (2020) 110765.
- [16] Assis M., Robeldo T., Foggi C.C., Kubo A.M., Mínguez-Vega G., Condoncillo E., Beltran-Mir H., Torres-Mendieta R., Andrés J., Oliva M., Vergani C.E., Barbugli P.A., Camargo E.R., Borra R.C., Longo E., ~~*Scientific Reports*~~, *Rep. Sci. Rep.* 9 (2019) 9927.
- [17] Macedo N.G., Machado T.R., Roca R.A., Assis M., Foggi C.C., Puerto-Belda V., Mínguez-Vega G., Rodrigues A., San-Miguel M.A., Cordoncillo E., Beltrán-Mir H., Andrés J., Longo E., *ACS Applied Bio Materials* 2 (2019) 824–837.
- [18] Sousa G.D., Nobre F.X., Araujo E.A., Sambrano J.R., Albuquerque A.D., Binda R.D., Couceiro P.R.D., Brito W.R., Cavalcante L.S., Santos M., de Matos J.M.E., *Arabian J. Chem.* 13 (2020) 2806–2825.
- [19] Liu X.T., Li W.J., Li H.D., Ren C.J., Li X.Y., Zhao Y.J., ~~*Appl. Catal. A A Gen.*~~, *Appl. Catal. A Gen.* 568 (2020) 54–63.
- [20] Wu M., Lv H.Y., Wang T., Ao Z.M., Sun H.Q., Wang C.Y., An T.C., Wang S.B., *Catal. Today* 315 (2020) 205–212.
- [21] Wang Z.L., Dai K., Liang C.H., Zhang J.F., Zhu G.P., *Mater. Lett.* 196 (2020) 373–376.
- [22]

- [23] Xu H., Cao Y.L., Xie J., Hu J.D., Li Y.Z., Jia D.Z., Mater. Res. Bull. 102 (2018) 342–352.
- [24] Li J.J., Yu C.Y., Zheng C.C., Etogo A., Xie Y.L., Zhong Y.J., Hu Y., Mater. Res. Bull. 61 (2015) 315–320.
- [25] Feizpoor S., Habibi-Yangjeh A., Mater. Res. Bull. 99 (2018) 93–102.
- [26] Li H.F., Li M.F., Chu Y., Liu F., Nie H., Fuel 116 (2014) 168–174.
- [27] Kuznetsov P.N., Kazbanova A.V., Kuznetsova L.I., Kovalchuk V.I., Mikhlin Y.L., ~~Reaction Kinetics Mechanisms and Catalysis. Kinet. Mech. Catal.~~React. Kinet. Mech. Catal. 113 (2014) 69–84.
- [28] Tobaldi D.M., Pullar R.C., Gualtieri A.F., Seabra M.P., Labrincha J.A., ~~Acta Materialia. Acta Mater.~~ 61 (2013) 5571–5585.
- [29] Kartsonakis I.A., Kordas G., ~~Journal of the American Ceramic Society. Am. Ceram. Soc. J. Am. Ceram. Soc.~~ 93 (2010) 65–73.
- [30] Patil P.R., Patil P.S., Thin Solid Films 382 (2001) 13–22.
- [31] Krtil P., Nishimura S., Yoshimura M., Electrochim. Acta 44 (1999) 3911–3920.
- [32] Malyshev V., Gab A., Popescu A.M., Constantin V., Revista De Chimie 62 (2011) 1128–1130.
- [33] Chen L.P., Gao Y.H., ~~Materials Chemistry and Physics. Chem. Phys. Mater. Chem. Phys.~~ 116 (2009) 242–246.
- [34] Thangaraju D., Durairajan A., Balaji D., Babu S.M., Hayakawa Y., ~~Journal of Luminescence. Lumin. J. Lumin.~~ 134 (2013) 244–250.
- [35] Jin J.J., Yang K.S., Su J.Y., Si Z.J., ~~Journal of Luminescence. Lumin. J. Lumin.~~ 159 (2015) 178–182.
- [36] Lebedev A.V., Avanesov S.A., Yunalan T.M., Klimenko V.A., Ignatyev B.V., Isaev V.A., ~~Optical Materials. Mater. Opt. Mater.~~ 52 (2016) 203–211.
- [37] Lv W.Z., Huang D.Z., Chen Y.M., Qiu Q., Luo Z.K., ~~Ceramics International. Int. Ceram. Int.~~ 40 (2014) 12661–12668.
- [38] De Santana Y.V.B., Gomes J.E.C., Matos L., Cruvinel G.H., Perrin A., Perrin C., Andres J., Varela J.A., Longo E., Nanomater. Nanotechnol. 4 (2014) 22–31.
- [39] Cavalcante L.S., Almeida M.A., Avansi W. Jr., Tranquilin R.L., Longo E., Batista N.C., Mastelaro V.R., Li M.S., Inorg. Chem. 51 (2012) 10675–10687.
- [40] Ocakoglu K., Mansour S.A., Yildirimcan S., Al-Ghamdi A.A., El-Tantawy F., Yakuphanoglu F., ~~Spectrochimica Acta Part a-Molecular and Biomolecular Spectroscopy. Biomol. Spectros.~~Spectrochimica Acta Part a-Mol. Biomol. Spectros. 148 (2015) 362–368.

- [41] Hu Y., Liu Y., Qian H.S., Li Z.Q., Chen J.F., *Langmuir* 26 (2010) 18570–18575.
- [42] Cunha F.S., Sczancoski J.C., Nogueira I.C., de Oliveira V.G., Lustosa S.M.C., Longo E., Cavalcante L.S., *Crystengcomm* 17 (2015) 8207–8211.
- [43] Silva M.D.P., Goncalves R.F., Nogueira I.C., Longo V.M., Mondoni L., Moron M.G., Santana Y.V., Longo E., *Spectrochim. Acta, Part A* 153 (2016) 428–435.
- [44] ~~Journal of large-scale research facilities. Large-scale Res. Facil. Jlsrf~~ [J. Large-scale Res. Facil. Jlsrf](#) 3 (2017) A103.
- [45] Laier L.O., Assis M., Foggi C.C., Gouveia A.F., Vergani C.E., Santana L.C.L., Cavalcante L.S., Andres J., Longo E., *Theor. Chem. Acc.* 139 (2020).
- [46] Roca R.A., Sczancoski J.C., Nogueira I.C., Fabbro M.T., Alves H.C., Gracia L., Santos L.P.S., de Sousa C.P., Andres J., Luz G.E. Jr., Longo E., Cavalcante L.S., *Catal. Sci. Techn.* 5 (2015) 4091–4107.
- [47] Dovesi R., Saunders V.R., Roetti C., Orlando R., Zicovich-Wilson C.M., Pascale F., Civalleri B., Doll K., Harrison N.M., Bush I.J., D'Arco P., Llunel M., Causà M., Noël Y., *CRYSTAL14 User's Manual*, Theoretical Chemistry Group, University of Turin, Italy, 2014.
- [48] Gualtieri A.F., Gatta G.D., Arletti R., Artioli G., Ballirano P., Cruciani G., Guagliardi A., Malferrari D., Masciocchi N., Scardi P., *Period. di Mineral.* 88 (2019) 147–151.
- [49] Larson A.C., Von Dreele R.B., ~~General structure analysis system (GSAS)~~ [General Structure Analysis System \(GSAS\)](#), Los Alamos: National Laboratory, 2001.
- [50] Longo E., Volanti D.P., Longo V.M., Gracia L., Nogueira I.C., Almeida M.A.P., Pinheiro A.N., Ferrer M.M., Cavalcante L.S., Andres J., *J. Phys. Chem. C* 118 (2014) 1229–1239.
- [51] Gouveia A.F., Sczancoski J.C., Ferrer M.M., Lima A.S., Santos M.R., Li M.S., Santos R.S., Longo E., Cavalcante L.S., *Inorg. Chem.* 53 (2014) 5589–5599.
- [52] Gupta S.K., Sudarshan K., Ghosh P.S., Mukherjee S., Kadam R.M., *J. Phys. Chem. C* 120 (2016) 7265–7276.
- [53] Moura J.V.B., da Silva J.G., Freire P.T.C., Luz-Lima C., Pinheiro G.S., Viana B.C., Mendes J., Souza A.G., Saraiva G.D., ~~Vibrational Spectroscopy. Speetrose.~~ [Vib. Spectrosc.](#) 86 (2016) 97–102.
- [54] Zhang R., Cui H., Yang X., Liu H., Tang H., Li Y., *Micro Nano Lett.* 7 (2012) 1285–1288.
- [55] Longo E., Cavalcante L.S., Volanti D.P., Gouveia A.F., Longo V.M., Varela J.A., Orlandi M.O., Andres J., *Sci. Rep.* 3 (2013) 1676.
- [56] Andres J., Ferrer M.M., Gracia L., Beltran A., Longo V.M., Cruvinel G.H., Tranquilin R.L., Longo E., ~~Part. Part. Syst. Char.~~ [Part. Part. Syst. Charact.](#) 32 (2015) 646–651.
- [57] Botelho G., Sczancoski J.C., Andres J., Gracia L., Longo E., *J. Phys. Chem. C* 119 (2015) 6293–6306.

- [58] de Oliveira R.C., Assis M., Teixeira M.M., da Silva M.D.P., Li M.S., Andres J., Gracia L., Longo E., J. Phys. Chem. C 120 (2016) 12254–12264.
- [59] Andres J., Gracia L., Gonzalez-Navarrete P., Longo V.M., Avansi W. Jr., Volanti D.P., Ferrer M.M., Lemos P.S., La Porta F.A., Hernandez A.C., Longo E., Sci. Rep. 4 (2014) 5391–5397.
- [60] Fabbro M.T., Saliby C., Rios L.R., La Porta F.A., Gracia L., Li M.S., Andres J., Santos L.P.S., Longo E., Sci. Technol. Adv. Mater. 16 (2015).
- [61] Longo V.M., De Foggi C.C., Ferrer M.M., Gouveia A.F., Andre R.S., Avansi W., Vergani C.E., Machado A.L., Andres J., Cavalcante L.S., Hernandez A.C., Longo E., J. Phys. Chem. A 118 (2014) 5769–5778.
- [62] Guettai N., Amar H.A., Desalination 185 (2005) 439–448.
- [63] Huang J.W., Jin B., Liu H.Q., Li X.J., Zhang Q.C., Chu S.J., Peng R.F., Chu S., J. Mater. Chem.

Graphical abstract



Highlights

- Synthesis of $\alpha\text{-Ag}_2\text{W}_{0.75}\text{Mo}_{0.25}\text{O}_4$ using CP method followed by microwave irradiation.
- Longest microwave irradiation time enhanced the material properties.
- Theoretical results from DFT calculations were compared with experimental data.

Appendix A Supplementary data

The following is Supplementary data to this article:

[Multimedia Component 1](#)

Queries and Answers

Query: Your article is registered as a regular item and is being processed for inclusion in a regular issue of the journal. If this is NOT correct and your article belongs to a Special Issue/Collection please contact v.manomohan@elsevier.com immediately prior to returning your corrections.

Answer:

Query: The author names have been tagged as given names and surnames (surnames are highlighted in teal color). Please confirm if they have been identified correctly.

Answer:

Query: Please note that Table 2 have been cited in the text but not provided. Please provided them or delete these citations from the text.

Answer:

Query: Have we correctly interpreted the following funding source(s) and country names you cited in your article: FAPEMA; CAPES; FAPESP and CNPq?

Answer:

Query:

Answer:

Query: Please check the year inserted by the copyeditor in reference [18,19,20,21 and 22] and correct if necessary.

Answer: